AGU PUBLICATIONS

JGR

Journal of Geophysical Research: Space Physics

RESEARCH ARTICLE
10.1002/2016JA023050

On the dynamics of large-scale traveling ionospheric disturbances over Europe on 20 November 2003

Claudia Borries[1], Norbert Jakowski[1], Kirsti Kauristie[2], Olaf Amm[2,3], Jens Mielich[4], and Daniel Kouba[5]

[1]Institute of Communications and Navigation, German Aerospace Center, Neustrelitz, Germany, [2]Arctic Research Centre, Finnish Meteorological Institute, Helsinki, Finland, [3]Deceased 16 December 2014, [4]Leibniz Institute of Atmospheric Physics, University of Rostock, Juliusruh, Germany, [5]Institute of Atmospheric Physics, Prague, Czech Republic

Key Points:
- The TID source region is characterized by strong ionospheric perturbations
- The TIDs are generated by Joule heating due to electrojet dissipation or particle precipitation
- The source region of the TID moves equatorward due to compression of the plasmasphere

Correspondence to:
C. Borries,
claudia.borries@dlr.de

Citation:
Borries, C., N. Jakowski, K. Kauristie, O. Amm, J. Mielich, and D. Kouba (2017), On the dynamics of large-scale traveling ionospheric disturbances over Europe on 20 November 2003, *J. Geophys. Res. Space Physics*, *122*, doi:10.1002/2016JA023050.

Received 10 JUN 2016
Accepted 3 JAN 2017
Accepted article online 7 JAN 2017

Abstract Ionospheric disturbances, often associated with geomagnetic storms, may cause threats to radio systems used for communication and navigation. One example is the super storm on 20 November 2003, when plenty of strong and unusual perturbations were reported. This paper reveals additional information on the dynamics in the high-latitude ionosphere over Europe during this storm. Here analyses of wavelike traveling ionospheric disturbances (TIDs) over Europe are presented, based on estimates of the total electron content (TEC) derived from ground-based Global Navigation Satellite System (GNSS) measurements. These TIDs are ionospheric signatures of thermospheric surges initiated by space weather events. The source region of these TIDs is characterized by enhanced spatial gradients, TEC depression, strong uplift of the F_2 layer, the vicinity of the eastward auroral electrojet, and strong aurora *E* layers. Joule heating is identified as the most probable driver for the TIDs observed over Europe during 20 November 2003. The sudden heating of the thermosphere leads to strong changes in the pressure and thermospheric wind circulation system, which in turn generates thermospheric wind surges observed as TID signatures in the TEC. Either the dissipation of the eastward auroral electrojet or particle precipitation are considered as the source mechanism for the Joule heating. In the course of the storm, the TEC observations show a southward shift of the source region of the TIDs. These meridional dislocation effects are obviously related to a strong compression of the plasmasphere. The presented results demonstrate the complex interaction processes in the thermosphere-ionosphere-magnetosphere system during this extreme storm.

1. Introduction

Severe perturbations in the electron density of the ionosphere are closely related to geomagnetic storms [e.g., *Jakowski et al.*, 1990; *Fuller-Rowell et al.*, 1994]. Many of these perturbations can impact the functioning of radio systems widely used for communication and navigation. To mitigate associated performance degradation, it is crucial to understand ionospheric perturbations during geomagnetic storms.

Large-scale traveling ionospheric disturbances (TIDs) occurring during geomagnetic storms have been a well-known phenomenon for decades [e.g., *Davis and Rosa*, 1969; *Maeda and Handa*, 1980; *Hunsucker*, 1982; *Jakowski and Putz*, 1986; *Kersley and Hughes*, 1989; *Hajkowicz*, 1991; *Hocke and Schlegel*, 1996; *Oliver et al.*, 1997; *Ho et al.*, 1998; *Ding et al.*, 2007; *Shiokawa et al.*, 2003; *Afraimovich et al.*, 2008; *Borries et al.*, 2009; *Shimeis et al.*, 2015]. They are the manifestation of atmospheric gravity waves (AGWs) originating in the auroral region due to thermospheric heating induced by storm-related perturbations. The ionosphere may act as a passive tracer to display the motion of the neutral atmosphere. Recently, the main properties of large-scale TIDs have been described in statistical studies for Japan [*Tsugawa et al.*, 2004], North America [*Ding et al.*, 2008], and Europe [*Borries et al.*, 2009]. However, the mechanisms producing large-scale TIDs during geomagnetic storms are still not clear. According to *Hajkowicz* [1991] and *Hunsucker* [1982], two processes are considered to be responsible for the generation of AGWs during a substorm: (1) the Lorentz force $(\vec{j} \times \vec{B})$ set up by the electric currents of the auroral electrojet and transferred to the neutral gas via collision in the *E* region; (2) the Joule heating $(\vec{j} \cdot \vec{E}) = j^2/\sigma_c$ of the neutral air by the electrojet or particle precipitation, where $\vec{j}$ and $\vec{B}$ are the current and magnetic field density, $\vec{E}$ is the electric field strength, and $\sigma_c = (\sigma_P^2 + \sigma_H^2)/\sigma_P$ is the Cowling conductivity of the ionosphere with Pederson conductivity σ_P and Hall conductivity σ_H. *Oyama and Watkins* [2012], who recently reviewed the latest research on these two processes, noted that there is a tendency for the wind velocity to

be correlated with the Lorentz force and for the temperature perturbation to be correlated with Joule heating. Both terms therefore come into play when AGWs are generated in the lower thermosphere. Finally, they pointed out that the contribution of Joule heating increases with altitude (up to a certain limit). The generation of AGW due to Joule heating was demonstrated by *Shiokawa et al.* [2007].

The principal factor in both processes is the intensity of the auroral electrojet. A key parameter closely related to the occurrence of TIDs during storm events thus seems to be the amplitude of the auroral electrojet index (*AE*). This assumption has been confirmed by *Ding et al.* [2008] and *Borries et al.* [2009]. The latter found a high correlation between the amplitudes of daytime TIDs over Europe during high solar activity and *AE*. Similarly, *Ding et al.* [2008] showed a dramatic increase of the occurrence rate of large-scale TIDs over North America with increasing *AE*, where at $AE = 2400$ nT the probability of the occurrence of large-scale TIDs exceeds 60%.

In this paper, TID characteristics and source mechanisms during the geomagnetic storm on 20 November 2003 are investigated. This storm is the largest geomagnetic storm in the 23rd solar cycle [*Gopalswamy et al.*, 2005] and one of the largest ever recorded. It has thus been widely discussed in the past [e.g., *Foster et al.*, 2005; *Kataoka et al.*, 2005; *Crowley et al.*, 2006; *Alex et al.*, 2006; *Hori et al.*, 2006; *Mishin et al.*, 2007; *Baishev et al.*, 2008]. Accordingly, extreme perturbations in the ionosphere during this storm event have been reported [e.g., *Jin et al.*, 2008; *Yizengaw et al.*, 2006; *Mayer et al.*, 2008; *Mannucci et al.*, 2008; *De Franceschi et al.*, 2008]. However, there has been no discussion of TID activity over Europe during this extreme storm event in particular. Our aim here is to present a comprehensive view on the dynamics in the thermosphere-ionosphere-magnetosphere system in the source region of the large-scale TIDs during the strong geomagnetic storm on 20 November 2003.

2. Data Base

Perturbations in the ionosphere are primarily detected by measurements of the total electron content (TEC). A dense network of Global Navigation Satellite System (GNSS) receivers over Europe enables the reliable TEC monitoring and characterization of large-scale TIDs. Maps of TID amplitudes are generated using the algorithms described by *Borries et al.* [2009], where the relative TEC is estimated along the line of sight between the satellite and receiver from the differential carrier phases. This relative slant TEC is roughly calibrated with the Neustrelitz TEC model [*Jakowski et al.*, 2011] and then converted with a mapping function by using a single-layer approximation of the ionosphere. The continuous TEC measurements between one satellite and one ground receiver are considered as the link. The TEC perturbation (TID) amplitudes are computed by subtracting a 1 h moving average from the link data. The resulting TEC perturbation data are mapped into a regular grid with the resolution of 1° in latitude and longitude and 1 min in time.

Large-scale TEC gradients are derived from European TEC maps that are routinely produced by the German Aerospace Center (DLR) [*Jakowski*, 1996]. These maps are computed from ground-based GNSS measurements provided by the International GNSS Service (IGS) and the European subcommission of the International Association of Geodesy (EUREF). Their resolution is 2.5° in latitude, 5° in longitude, and 30 min in time. The TEC amplitude is measured in TEC units (1 TECU $= 10^{16}$ electrons/m^2). Temporal gradients are computed from two subsequent TEC maps. The absolute spatial TEC gradient $||\nabla \mathrm{TEC}||_2 := \sqrt{|\frac{\partial \mathrm{TEC}}{\partial \mathrm{lat}}|^2 + |\frac{\partial \mathrm{TEC}}{\partial \mathrm{lon}}|^2}$ is computed from the latitudinal and longitudinal gradients extracted from a TEC map. The significance was estimated by calculating the temporal and spatial gradients for the whole year 2003. Gradients are considered as 95% significant, if their amplitude is larger than 97.5% of the 2003 gradients or lower than 97.5% of the 2003 gradients. The spatial and temporal TEC gradients are used as indicators for large-scale disturbance zones, while the TEC perturbation amplitudes described above predominantly indicate perturbations of smaller scales like the TIDs.

Estimations of the polar electrojets are derived from measurements by the International Monitor for Auroral Geomagnetic Effects (IMAGE) magnetometer network [*Viljanen and Häkkinen*, 1997]. IMAGE currently consists of 35 magnetometer stations (Figure 1, not all 35 stations were available in 2003) maintained as collaboration of several European institutes. The prime objectives of IMAGE are to study auroral electrojets and dynamic two-dimensional current systems. Here magnetometer measurements from Finland are used to show the electrojet location.

The electrojet index (*IE*), derived from the IMAGE magnetometers, is used complementary to the auroral electrojet index (*AE*). Although, *IE* is not able to show the storm in its full power during morning hours

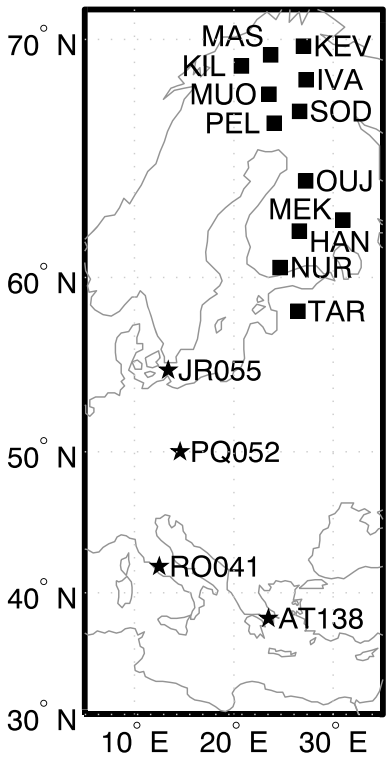

Figure 1. Location of the IMAGE magnetometers (squares) and ionosonde stations (stars) used for the presented analyses.

(as the magnetometer chain is not scanning the midnight sector), it presents the local geomagnetic disturbances in northern Europe well. In this case study, *IE* recorded higher values because, with its low-latitude stations, IMAGE captures activity in the expanded oval more accurately than the standard *AE* chain. Additionally, the disturbance storm index *Dst* and the *SYM-H* index are presented to allow the characterization of the storm phases.

Based on a simple linear model described by *Prölss* [2006], we estimate the location of the trough region. Here we assume the trough to be located in the vicinity of the Subauroral Electron Temperature Enhancement (SETE). The model simply describes a linear relation between *Dst* and the magnetic latitude (mlat) of the SETE.

$$\text{mlat} = a + b \cdot Dst \tag{1}$$

In this model $a = 60.7$ and $b = 0.08$ [*Prölss*, 2006] have been used.

Vertical sounding measurements are presented from the ionosonde stations Juliusruh, Pruhonice, Rome, and Athens. Their locations are shown on the map in Figure 1.

3. Observations

To characterize the magnetic storm of 20 November 2003, Figure 2 shows the *Dst* index, *SYM-H* component, the electrojet index *IE*, and the auroral electrojet index *AE* (first and second panels). This storm had a rapid onset, i.e., a fast increase of *Dst* and *SYM-H* at 8 UT and a steep decrease to the minimum *Dst* value of −422 nT. The *AE* rapidly increased from 522 nT to 1129 nT. The maximum *AE* value during the storm was 1517 nT, reached at 13 UT. The *IE* showed only a short but rapid increase at the storm onset and reached its maximum value of 2000 nT at 15 UT. There were two times during the storm when the *AE* decreased for a short while. At 12 UT *AE* had only 570 nT and at 14 UT it was only 643 nT. The storm onset time is assumed to be at 8 UT, when *AE* and *Dst* suddenly increased.

Figure 2 (third panel) demonstrates the TID activity, indicating the amplitude of the perturbations through the color code. It is interesting to note that a weak meridional pattern occurs at storm onset around 08:00 UT in Figure 2. This immediate response at all latitudes from about 60°N southward occurs at the same time as the sudden increase of *SYM-H* and the peak of *IE* (cf. first and second panels). This perturbation pattern is followed by slanted TEC perturbation signatures. The slope of this amplitude pattern toward lower latitudes (slanted rays) clearly indicates the presence of equatorward propagating TIDs. The first TID starts at about 10 UT at 60°N, propagates equatorward with a speed of 629 ± 48 m s^{-1} [*Borries et al.*, 2009] and reaches 40°N latitude at about 11 UT. Several other TIDs with a period of approximately 1 h follow in the subsequent hours. Interestingly, the later TIDs do not start at 60°N like the first TID. Their onset region shifts equatorward. The last TID at 17 UT starts at about 43°N. The white line in this plot (and also in the following plots) indicates the approximate start region of the TIDs. This white line is actually the approximate location of the ionospheric midlatitude trough region according to the trough model described in the previous section. Large perturbation amplitudes can be found north of the TID start region. Their amplitudes exceed 2 TECU. Since they do not show a clear slope or structure, we refer to them not as TIDs but as polar electron density patches.

Figure 2 (fourth panel) shows the spatial TEC gradients derived from DLR TEC maps. Black lines encapsulate wave amplitudes detected with 95% significance. Maximum gradients are located exactly in the start region of the TIDs (white line) with amplitudes of 0.02 TECU/km (also having 95% significance level).

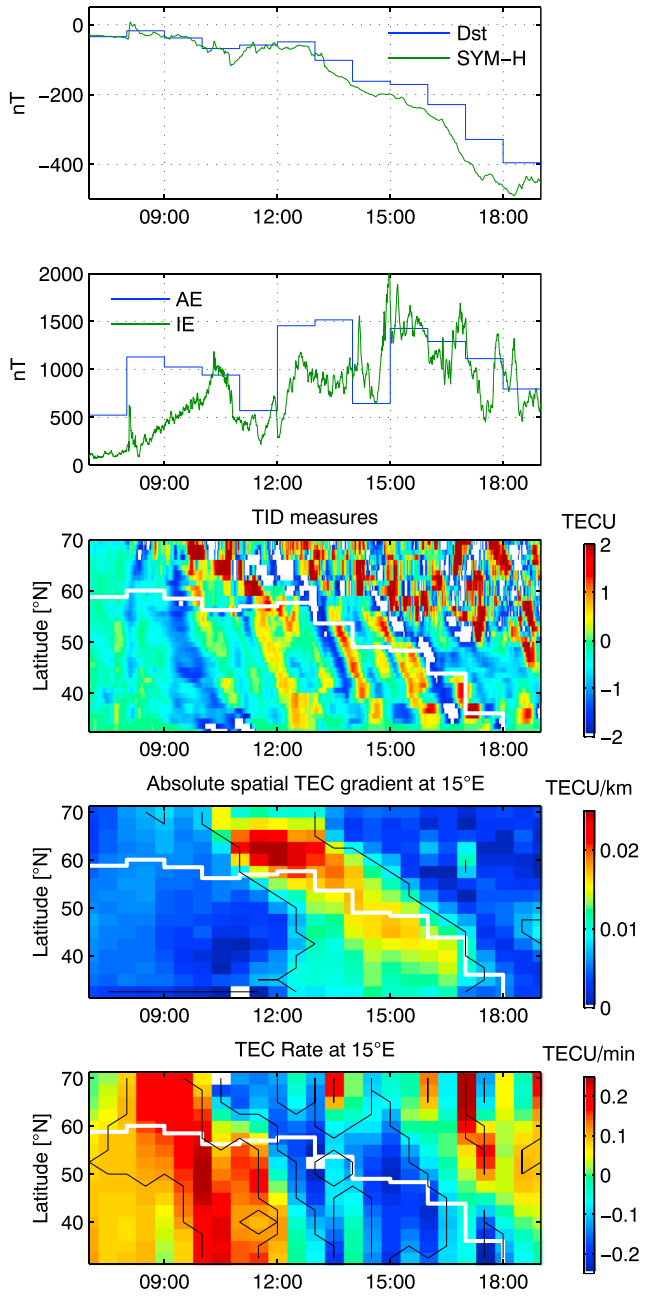

Figure 2. (first panel) *Dst* index (blue) and *SYM-H* component (green) on 20 November 2003. (second panel) Auroral electrojet index *AE* (blue) and electrojet index *IE* (green). (third panel) Time-latitude plot of TID estimates (TEC deviations to the 1 h moving average) at 15°E, (fourth panel) spatial TEC gradients derived from DLR TEC maps at 15°E, (fifth panel) TEC rate derived from DLR TEC maps at 15°E. The white line approximates the trough location.

Analogous to Figure 2 (fourth panel), Figure 2 (fifth panel) shows the TEC rate derived from DLR TEC maps. Again, amplitudes with 95% significance are encapsulated by black lines. A strong enhancement of the TEC with up to 0.2 TECU/min is observed right after the storm onset. It starts in high latitudes at around 8:30 UT and appears slightly later in midlatitudes. At 32.5°N (lower bound of the plot) the significant TEC enhancement starts at 10:00 UT. Subsequent to the TEC enhancement, a TEC depletion with a 95% significance and an amplitude of −0.2 TECU/min is observed. It appears during the southward shift of the TID start region indicated by the white line.

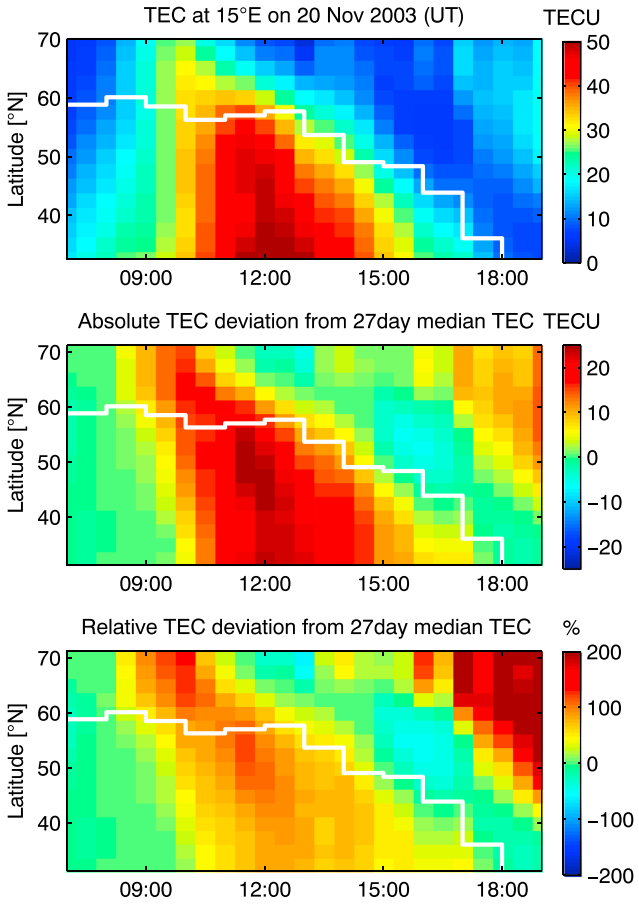

Figure 3. (top) Latitude-time plot of TEC derived from DLR TEC maps at 15°E on 20 November 2003. (middle) Latitude-time plot of absolute TEC deviations to 27 days median TEC derived from DLR TEC maps at 15°E. (bottom) Latitude-time plot of percentage TEC deviations to 27 days median TEC derived from DLR TEC maps at 15°E.

In relation to the TIDs and TEC gradients shown in Figure 2, Figure 3 (top) displays the TEC observations and absolute and percentage TEC deviations to quiet conditions (Figures 3, middle and 3, bottom) extracted from DLR TEC maps. Here the median TEC of the preceding 27 days is used to estimate quiet TEC conditions. During daytime, the TEC increases to more than 50 TECU in middle and lower latitudes. This is about 25 TECU more than the median of the preceding 27 days and an increase by 100%. The minimum TEC in the evening hours can be found 5 to 10° north of the TID start region. It is located at 60°N at 15 UT and subsequently shifts equatorward. At 18 UT it is at 40°N. This seems to be the actual center of the midlatitude trough. In the trough region, there is little deviation from the 27 day median. Here the TEC is 0 to 5 TECU lower than the median TEC. After 15 UT, poleward of the trough region, the TEC increases to up to 18 TECU. This is an increase by more than 10 TECU, or more than 200%. As will be discussed later, this enhancement probably has major contributions from the plasma transport from the American sector, as indicated in polar plots presented in *Jakowski et al.* [2007].

For comparison, ionosonde measurements from 20 November 2003 are displayed in Figure 4. The critical frequency f_oF_2 (blue dots) and the peak electron density height h_mF_2 (red dots) are shown for Juliusruh (JR055), Pruhonice (PQ052), Rome (RO041), and Athens (AT138). All stations indicate a strong increase of f_oF_2 until noon and a sharp decrease of f_oF_2 in the afternoon. At all stations, the increase in the morning and the decrease in the afternoon are not monotonical. Individual perturbations are observed, probably due to the passage of TIDs. Small time differences in the periods when TIDs are passing above individual ionosonde stations (Figure 4), compared with the times in Figure 2, may be caused by a slightly different longitude of the station and longitude for Figure 2 (15°E). After the observation of the primary f_oF_2 peak, the decrease starts at 11:45 UT in Juliusruh, at about 12:25 UT in Pruhonice, at about 13:00 UT in Rome, and at about 12:30 UT in Athens. The h_mF_2 is quite constant during the day at all stations. But in the afternoon, it suddenly increases

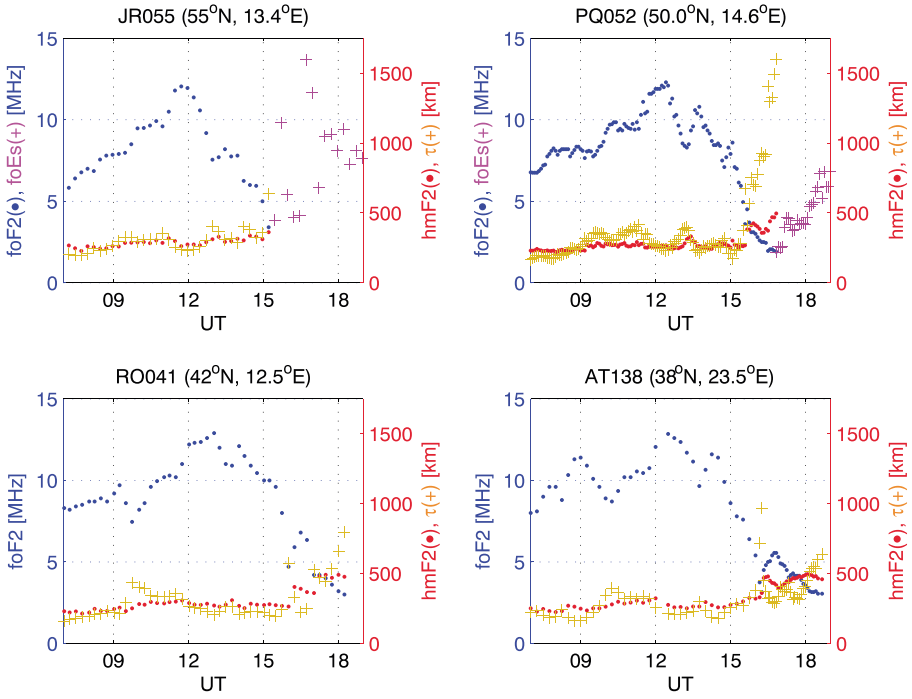

Figure 4. Sharp gradients measured during 20 November 2003 in the F_2 layer peak height (h_mF_2, red bullets), the equivalent slab thickness (τ, orange crosses), and the critical frequency (f_oF_2, blue bullets) at the ionosonde station Athens (AT138), Rome (RO041), Pruhonice (PQ052), and Juliusruh (JR055). The Aurora *E* layer critical frequency (*foEs*, magenta crosses) is shown for Juliusruh after 15 UT and Pruhonice after 16:30 UT.

significantly at all stations. In Pruhonice, it rises at 15:35 UT from 268 km to 382 km within 5 min. At 16:50 UT the F_2 layer is at an altitude of 496 km. In Rome, h_mF_2 increases at 16:01 UT from 264 km to 404 km within 15 min. The maximum measured altitude is 491 km at 18:01 UT. In Athens, h_mF_2 increases at 16:15 UT from 360 km to 468 km within 15 min. The maximum measured altitude is 496 km at 18:05 UT. The sharp increase of h_mF_2 could not be measured in Juliusruh. At the time of the expected increase, the *E* layer electron density (aurora *E* layer, magenta crosses in Figure 4) suddenly increases significantly. This effect prevented the measurement of the F_2 layer. The same effect causes the missing measurements after 16:50 UT in Pruhonice.

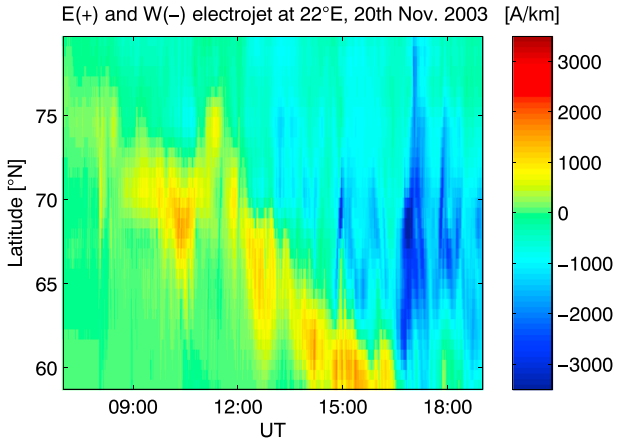

Figure 5. IMAGE ionospheric equivalent currents in west-east direction on 20 November 2003. They indicate the location of the Auroral electrojets. For each time step the latitude profile along the middle meridian of the 2-D current map (along 22°E) is shown in the latitude-versus-time plots. Red colors (positive numbers) mean eastward equivalent currents, blue colors (negative numbers) mean westward currents.

The equivalent slab thickness τ, which is the ratio between the TEC and the peak electron density of the local ionosphere N_mF_2, is derived from the ionosonde measurements and DLR TEC maps. It is a measure of the width of the shape of the vertical electron density profile of the ionosphere. The τ estimates shown in Figure 4 (orange plus signs) are between 200 and 400 km before 15 UT at all four stations. After 15 UT all four stations show a strong increase of τ. Thus, τ exceeded 600 km at 15:15 UT at Juliusruh (with only occasional measurements due to the aurora *E* layer). A few minutes later, at approximately 15:30 UT, τ at Pruhonice started to increase dramatically. It reached 1600 km at 16:50 UT. In Rome and Athens, the slab

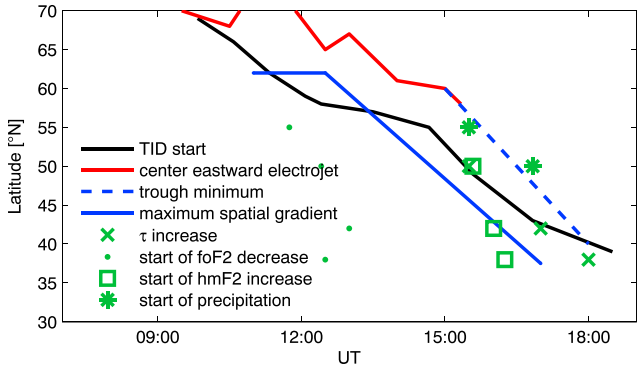

Figure 6. Schematic overview on the time and location of the approximate TID start region (black line), the approximate center of the eastward electrojet (red solid line), the center of the midlatitude trough (blue dashed line), the maximum spatial gradients (blue solid line), the sudden increase of slab thickness τ (green crosses), the start of f_oF_2 decrease (green dots), the start of h_mF_2 increase (green squares), and the start of precipitation (green asterisks), estimated from Figures 2–5.

thickness τ varies strongly after 16 UT. Still, at 18 UT it exceeds 600 km. Singular high values of τ are observed in Rome at 16 UT and in Athens at 16:30 and 16:45 UT. These are regarded as artifacts due to the strong gradients in f_oF_2, which cannot be reflected by the TEC maps, as they only have a 30 min temporal resolution.

The ionospheric equivalent currents [*Pulkkinen et al.*, 2003; *Amm and Viljanen*, 1999] calculated from the IMAGE ground magnetometers are shown in Figure 5. The actual ionospheric current system (which may be three dimensional), flowing within the ionospheric *E* layer at around 100 km altitude, causes magnetic field fluctuations on the ground that are measured by magnetometers. These fluctuations are used to estimate the ionospheric equivalent currents, which are not necessarily equal to the actual currents, but still provide a good estimate of the auroral electrojets' location. The eastward electrojet is indicated by a positive current and the westward electrojet by a negative one. During daytime, strong eastward currents are present. The intensification of the eastward current started at about 8:30 UT. At this time, the strongest current is observed at about 70°N. In the following hours, the location of the peak eastward currents shifted equatorward. At 15 UT, the center of the eastward electrojet reached 60°N. At about 16:30 UT the intensity of the westward current increased significantly.

Figure 6 shows a schematic overview of the time and location of the approximate TID start region (black line), the approximate center of the eastward electrojet (red solid line), the center of the midlatitude trough (blue dashed line), the maximum spatial gradients (blue solid line), the sudden increase of slab thickness τ (green crosses), the start of the f_oF_2 decrease (green dots), the start of the h_mF_2 increase (green squares), and the start of precipitation (green asterisks), estimated from Figures 2–5. It clearly demonstrates the close vicinity of all effects.

4. Discussion

As observed during many previous storms, large-scale TIDs occurred in midlatitudes over Europe during the superstorm on 20 November 2003 as well. Many wave trains were observed in the time between 10 and 17 UT (Figure 2). The amplitude of these wave trains is not constant during this time. While the first one between 10 and 11 UT has a low amplitude of roughly 0.5 TECU, the second at 11 to 12 UT has a higher amplitude of about 1 TECU. The third wave train at 13 UT is weak again and the fourth at 14 UT is strong. The varying amplitude of the TIDs can be related to the varying strength of the auroral electrojet [*Ding et al.*, 2008; *Borries et al.*, 2009]. However, a clear correlation between the TID amplitude and *AE* or *IE* cannot be identified in Figure 2.

Around 8:00 UT we see TEC perturbations equal at all latitudes from 60°N down to the lower boundary of the TID map in Figure 2. Figure 7 is introduced for better illustration of this perturbation. It shows the relative TEC measurements (left column) from which the TEC perturbations (right column) are derived for four GNSS stations at different latitudes. In agreement with Figure 2, a TEC depletion by 1 TECU is visible at about 8:00 UT at all stations below 60°N. This feature is not attributed to surges but to electric field effects which were probably restricted during daytime to the onset phase before the ring current was developed. Figure 8 shows solar wind measurements indicating the arrival of fast solar wind with high dynamic pressure at 8:03 UT. The IMAGE

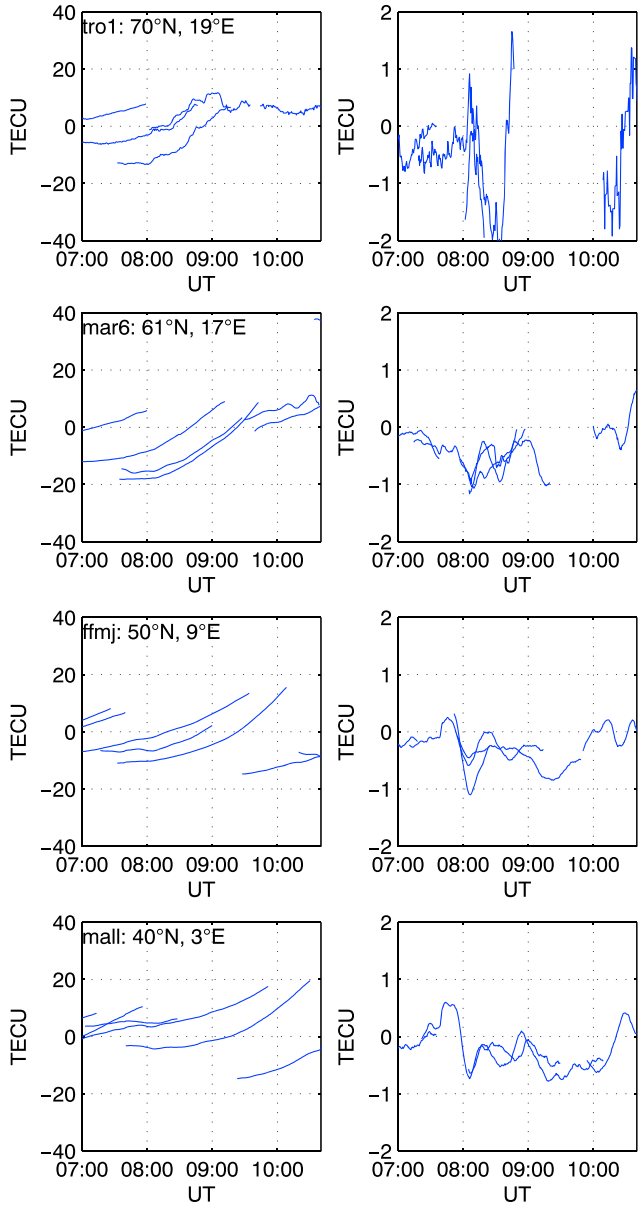

Figure 7. Demonstration of the (right column) filter response to a (left column) sudden depletion in the relative TEC measurements on 20 November 2003. The individual lines in the plots describe the measurements from one station to different satellites at the same time. Results are shown for the following GNSS stations from top to bottom: tro1, mar6, ffmj, and mall. A simultaneous TEC depletion is visible for the stations mar6, ffmj, and mall.

electrojet index *IE* indicates the sudden intensification of the eastward electrojet. Figure 8 (bottom) demonstrates that the eastward electrojet is strongest at this time at 70°N. Convection electric field effects are a suggested cause of the ionosphere and magnetosphere perturbations at 8:03 UT. TEC perturbations caused by an electric field effect have been shown earlier during severe storms [*Jakowski et al.*, 1992, 1999; *Arbesser-Rastburg and Jakowski*, 2007]. During the afternoon and evening hours, a very low *Dst* index indicates a strong ring current. During this time, electric field effects are limited to the polar cap region, e.g., by driving the auroral electrojet resulting in Joule heating and by the $E \times B$ drift of ionospheric plasma.

In the vicinity of the TID source region, enhanced large-scale spatial TEC gradients and a sudden TEC depletion are observed (Figure 2). The measured amplitude of 0.04 TECU/km is not very large compared to steep gradients observed by [*Mayer et al.*, 2008] with 1.2 TECU/km near Iceland during this same event. However, in contrast to these localized gradients, which were estimated directly from GNSS link data, the gradients shown

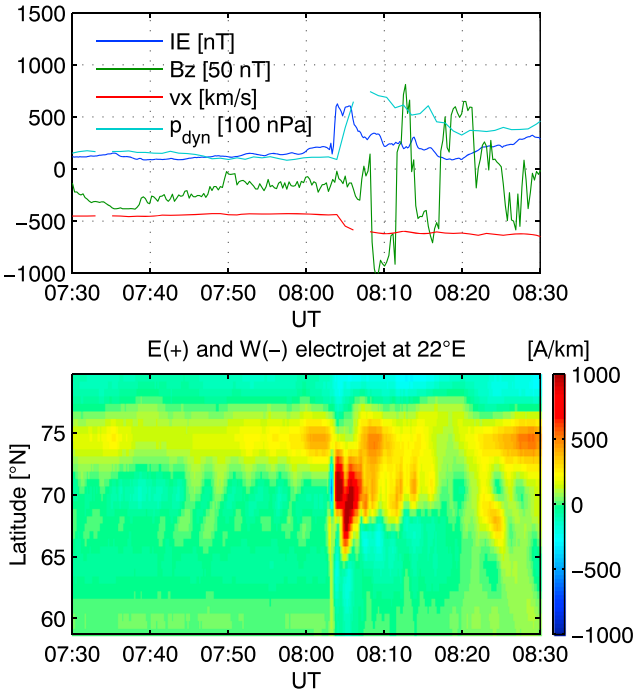

Figure 8. The IMAGE electrojet index (*IE*, dark blue), together with solar wind measurements from ACE: interplanetary magnetic field B_z component (green), solar wind speed v_x component (red), and solar wind dynamic pressure (light blue). The solar wind measurements are shifted by 37 min according to the time the solar wind (approx. 680 km/s) needs to arrive at Earth.

here are large scale. It should be noted that our gradients are derived from TEC maps where the mapping technique causes some smoothing of spatial structures. On the other hand, the structures are detected with 95% significance levels which confirms their authenticity.

Strong gradients are also seen in ionosonde measurements. The F_2 layer critical frequency (f_oF_2, Figure 4, blue bullets), which is proportional to the square root of the maximum electron density in the F_2 layer, shows a sharp decrease. The steepest gradient of f_oF_2 is hard to detect because of strong fluctuations, which can be associated with the passage of TIDs (most visible in Pruhonice PQ052). However, it seems to coincide with the maximum of the TEC gradients. Furthermore, the observed strong gradients in the TEC and f_oF_2 are accompanied by an unusual strong enhancement of h_mF_2. However, the increase of h_mF_2 does not coincide with the TID start region, because in lower latitudes the increase of h_mF_2 starts more than one hour before the passage of the TID start region. The equivalent slab thickness τ also revealed a dramatic increase. Here τ increased rapidly by more than 300 km or more than 100% within 1 h. In Pruhonice, τ even exceeded 1600 km. The τ increase seems to be located exactly in the TID starting region.

The described gradients demonstrate strong dynamics in the start region of the TIDs. The decrease of the plasma density (shown by f_oF_2) and the change of the profile shape shown by the increase of τ and h_mF_2 indicate intensive plasma transport with strong vertical components. Strong Joule heating in the auroral oval latitudes can cause an expansion of the thermosphere, triggering plasma upflow in the ionosphere. The location of the electrojets in Figure 5 and the observation of strong auroras by the Kilpisjärvi auroral camera (not shown here) indicate that the TID start region is in the auroral oval. The observed sudden dramatic increase of the equivalent slab thickness τ up to extreme heights like 1600 km, is seen as an indicator for that plasma upflow due to Joule heating. The report of a strong spread *F* at 15:13 UT Juliusruh (observed in the ionogram not shown here), which is related to strong gradients, fits the characteristics of strong heating, too. In case of spread *F*, the ionosphere is not evenly layered and plasma turbulences do occur. This leads to recordings of ionospheric echoes with multiple angles of arrival coming from all sky directions. However, spread *F* can be related either to the heating effect or precipitation effects.

An ion upflow mechanism as described in *Semeter et al.* [2003] is not considered as the source mechanism for the plasma transport in the TID source region, because this mechanism occurs at the polar cap boundary which is north of the TID source region.

Hence, thermal expansion should be considered as a strong mechanism exciting the observed TIDs. According to the theory described by *Volland* [1983], Joule heating in high latitudes leads to the development of two storm wind cells (one in each hemisphere). These storm wind cells are characterized by vertical upward winds in the heating region, meridional equatorward winds in the midlatitude *F* region, vertical downward winds at the end of the wind cell in middle to lower latitudes (the wind cell expands during the course of the storm toward the equatorial region), and poleward winds in altitudes below the height of maximum heat input. The effect of thermospheric expansion in the vicinity of the heat source transports heavier molecules (O_2, N_2) to greater altitudes where they cause an increase in the recombination rate. The electron density in the bottom side ionosphere and TEC decreases significantly and the F_2 layer height increases. This agrees with the assumption that the heating source is located northward of the TEC and f_oF_2 gradients. The heating region will have the lowest TEC. This is the case northward of the TID start region, in the midlatitude trough. In the heating region, we assume the presence of strong currents. At least at 15 UT, we can show the coincidence of the ionospheric trough and the eastward current at 60°N. Finally, the wind surges start at the equatorward boundary of the assumed heating region. This is shown via the observation of TIDs. While at noon the TIDs start roughly at the location of the steepest gradients of the TEC and f_oF_2, in the afternoon they start closer to the trough minimum. Sudden thermospheric expansion in the heating region thus seems to be a likely excitation mechanisms for the observed TIDs.

It is common knowledge that the high-latitude heat source drives global wind surges [e.g., *Prölss*, 1995]. The meridional winds transport the plasma upward along the magnetic field lines into altitudes with a lower recombination rate. In Figure 3, meridional equatorward winds are indicated by enhancements of the TEC and f_oF_2 in midlatitudes. In agreement with our knowledge that uplifting by meridional winds maximizes at around 45° magnetic latitude [*Förster and Jakowski*, 2000], we observe maximum TEC enhancement between 40°N and 50°N. The delayed increase with decreasing latitude also supports this idea. Meridional winds over Europe on 20 November 2003 at daytime were also presented by *Yizengaw et al.* [2006]. Additionally, model studies in *Crowley et al.* [2006], reproducing strong transport processes from high to midlatitudes during this storm event, support the assumption of thermospheric meridional winds. Using the Thermosphere-Ionosphere-Mesosphere-Electro Dynamics General Circulation Model (TIME-GCM), they show a transport of the ionospheric plasma to greater altitudes over Europe during noon (12 UT), where the ratio of production to loss is greater. They estimated that neutral winds are the main contributor to this effect. However, at noon h_mF_2 was below 300 km (roughly 20% above quiet values) at all ionosonde stations. A westward electric field generated by the disturbance dynamo (as described by *Yizengaw et al.* [2006]) might have reduced the uplift of the plasma. Downward transport of light oxygen at the equatorward end of the storm wind cell (in the middle to lower latitudes) probably enhanced the [O/N_2] ratio leading to increased electron density, while the F_2 layer remained at a relatively low altitude (compared to other storms). Again, the existence of meridional winds supports the assumption that the TIDs are generated by sudden thermospheric expansion.

Very characteristic in the TID observation in this case study is an equatorward displacement of the start region. Such a shift of the origin of large-scale TIDs to higher midlatitudes has already been reported by *Hajkowicz* [1991] for the great storm of 13 March 1989. He associated the shift with the magnitude of the disturbance, i.e., with the well-known property of the auroral oval to expand equatorward during large magnetic activity. In good agreement, the trough model by *Prölss* [2006], which assumes linear equatorward expansion with increasingly negative *Dst* values, works nicely in our case as the TID origin region closely follows the shift of the trough to lower latitudes (Figure 2, white line). Since the eastward electrojet is shifting similarly, this supports the relation of the TID origin to the shifting auroral oval. The auroral oval shifts because of strong electrodynamic coupling with the magnetosphere. An intensive compression of the plasmasphere, which is affecting the trough location [*Yizengaw and Moldwin*, 2005], has been shown for the superstorm of 20 November 2003 by *Bortnik et al.* [2006]. The compression reached its maximum around 18:00 UT (plasmapause at roughly two L shell). Furthermore, thickening of magnetospheric lobes is related to a decreasing latitude of the polar cap boundary. *Ebihara et al.* [2005] demonstrated the estimation of the polar cap boundary latitude based on Defense Meteorological Satellite Program Flight 13 (DMSP F13) measurements. They showed that the polar

cap boundary latitude decreased significantly during the storm main phase and reached an unusually low value of 60° MLAT at ≈16 UT on 20 November 2003.

The relocation of the auroral zone is also apparent in the ionosonde measurements. Enhanced aurora *E* layers (crosses in Figure 4) were reported at Juliusruh (15:15 UT) and Pruhonice (16:50 UT). They indicate the expansion of the auroral oval down toward the midlatitudes and can be explained by the precipitation of high energetic particles. *Blanch et al.* [2005] described in detail the precipitation effect observed in the ionograms over Europe during this storm event. Since precipitation starts at the plasmapause footprints (trough region), the record of precipitation effects is in agreement with the hypothesis that the observed TIDs are excited at the equatorward border of the trough region and that the shift of the start region of the TIDs occurred due to the compression of the plasmasphere.

As already mentioned, the TID start region is very close to the center of the eastward electrojet (Figure 5). According to the described extension of the auroral oval, we expect a further equatorward replacement of the eastward electrojet after 15 UT, which could not be measured by the IMAGE magnetometer network. About 30 years ago, *Crowley and Williams* [1987], *Williams et al.* [1988], and *Rice et al.* [1988] in a case study based on observations during the Worldwide Atmospheric Gravity Wave Study (WAGS) campaign, already described that auroral disturbances with clear periodicities in the electric field variations were followed by TIDs. Their findings lead us to suggest that in our case the dissipation of auroral currents also caused the heating that excited large-scale AGWs. In good agreement, a varying intensity of the equivalent currents is visible in Figure 5. However, it is hard to find a correlation between the periods in the current intensity and the TIDs. Next to the currents, strong precipitation effects have also been shown in the TID start region. Heating due to precipitation is a second potential mechanism providing an efficient heat source for the generation of large-scale AGWs. On average, Joule heating rates are larger than particle heating rates because of their extent over larger areas of the ionosphere and longer duration. But the particle heating rate can temporarily exceed the Joule heating rate [*Oyama and Watkins*, 2012; *Crowley and Williams*, 1987]. More studies are necessary, e.g., with physics-based models, to gain more knowledge on the source mechanism of the observed TIDs and perturbations.

5. Summary and Conclusions

The superstorm on 20 November 2003 caused extreme perturbations in the thermosphere-ionosphere-magnetosphere system. Here the observation of TIDs has been discussed in relation to other perturbations in the thermosphere-ionosphere-magnetosphere system that have been reported previously.

Several TID signatures have been identified on 20 November 2003, which start shortly after the onset of the storm. The TID start region, which is clearly visible in the TEC observations, is characterized by strong perturbations in the ionosphere. The observations revealed strong TEC gradients, the vicinity of the midlatitude ionospheric trough, gradients in f_oF_2 and h_mF_2, precipitation effects, the vicinity of the eastward auroral electrojet, and a very strong increase in the equivalent slab thickness. Furthermore, a rapid equatorward shift of the auroral oval and ionospheric trough resulting from the strong compression of the plasmasphere was associated with a similar shift in the TID origin region. Heating effects have been identified to be the most probable driver for the disturbances observed during the 20 November 2003 storm and especially for thermospheric wind surges which are observed as TID signatures in the TEC. The sudden heating of the thermosphere leads to strong changes in the pressure and thermospheric wind circulation system, which in turn generate thermospheric wind surges causing the observed TID signatures in the TEC.

Since the presented results show the presence of the eastward auroral electrojet as well as indicators for precipitation effects in the start region of the TIDs, we expect one of the two phenomena to cause efficient heating, generating the AGWs that were presented in the TEC measurements. Further studies are necessary to find more information on the source mechanisms for the observed TIDs. Modeling studies might provide more details.

Acknowledgments
Our acknowledgment goes to the IMAGE team for providing the magnetometer data and the analyses on the equivalent currents (http://space.fmi.fi/image/beta/), to the International GNSS Service (IGS) and Federal Agency for Cartography and Geodesy (BKG) for providing the GNSS data used to generate the TEC maps and TID estimations (https://igs.bkg.bund.de/), to the World Data Center in Kyoto for providing the *Dst* index and *AE* index (http://wdc.kugi.kyoto-u.ac.jp/wdc/Sec3.html), and to SPIDR for providing the ionosonde data for Athens and Rome (http://spidr.ionosonde.net/spidr/).

References

Afraimovich, E., S. Voeykov, N. Perevalova, and K. Ratovsky (2008), Large-scale traveling ionospheric disturbances of auroral origin according to the data of the GPS network and ionosondes, *Adv. Space Res.*, *42*(7), 1213–1217, doi:10.1016/j.asr.2007.11.023.

Alex, S., S. Mukherjee, and G. Lakhina (2006), Geomagnetic signatures during the intense geomagnetic storms of 29 October and 20 November 2003, *J. Atmos. Sol. Terr. Phys.*, *68*(7), 769–780, doi:10.1016/j.jastp.2006.01.003.

Amm, O., and A. Viljanen (1999), Ionospheric disturbance magnetic field continuation from the ground to the ionosphere using spherical elementary current systems, *Earth Planets Space*, *51*, 431–440.
Arbesser-Rastburg, B., and N. Jakowski (2007), Effects on satellite navigation, in *Space Weather—Physics and Effects*, edited by V. Bothmer and I. A. Daglis, pp. 383–402, Springer, Berlin, doi:10.1007/978-3-540-34578-7_13.
Baishev, D., G. Borisov, V. Velichko, S. Samsonov, and K. Yumoto (2008), Variations in the geomagnetic field and auroras during the main phase of a large magnetic storm of November 20, 2003, *Geomagn. Aeron.*, *48*(2), 201–208, doi:10.1134/S0016793208020096.
Blanch, E., D. Altadill, J. Boška, D. Burešová, and M. Hernández-Pajares (2005), November 2003 event: Effects on the Earth's ionosphere observed from ground-based ionosonde and GPS data, *Ann. Geophys.*, *23*(9), 3027–3034, doi:10.5194/angeo-23-3027-2005.
Borries, C., N. Jakowski, and V. Wilken (2009), Storm induced large scale TIDs observed in GPS derived TEC, *Ann. Geophys.*, *27*(4), 1605–1612, doi:10.5194/angeo-27-1605-2009.
Bortnik, J., R. M. Thorne, T. P. O'Brien, J. C. Green, R. J. Strangeway, Y. Y. Shprits, and D. N. Baker (2006), Observation of two distinct, rapid loss mechanisms during the 20 November 2003 radiation belt dropout event, *J. Geophys. Res.*, *111*, A12216, doi:10.1029/2006JA011802.
Crowley, G., and P. J. S. Williams (1987), Observations of the source and propagation of atmospheric gravity waves, *Nature*, *328*, 231–233, doi:10.1038/328231a0.
Crowley, G., et al. (2006), Global thermosphere-ionosphere response to onset of 20 November 2003 magnetic storm, *J. Geophys. Res.*, *111*, A10S18, doi:10.1029/2005JA011518.
Davis, M., and A. D. Rosa (1969), Traveling ionospheric disturbances originating in the auroral oval during polar substorms, *J. Geophys. Res.*, *74*, 5721–5735.
De Franceschi, G., L. Alfonsi, V. Romano, M. Aquino, A. Dodson, C. N. Mitchell, P. Spencer, and A. W. Wernik (2008), Dynamics of high-latitude patches and associated small-scale irregularities during the October and November 2003 storms, *J. Atmos. Sol. Terr. Phys.*, *70*(6), 879–888, doi:10.1016/j.jastp.2007.05.018.
Ding, F., W. Wan, B. Ning, and M. Wang (2007), Large-scale traveling ionospheric disturbances observed by GPS total electron content during the magnetic storm of 29–30 October 2003, *J. Geophys. Res.*, *112*, A06309, doi:10.1029/2006JA012013.
Ding, F., W. Wan, L. Liu, E. Afraimovich, S. Voeykov, and N. Perevalova (2008), A statistical study of large-scale traveling ionospheric disturbances observed by GPS TEC during major magnetic storms over the years 2003–2005, *J. Geophys. Res.*, *113*, A00A01, doi:10.1029/2008JA013037.
Ebihara, Y., M.-C. Fok, S. Sazykin, M. F. Thomsen, M. R. Hairston, D. S. Evans, F. J. Rich, and M. Ejiri (2005), Ring current and the magnetosphere-ionosphere coupling during the superstorm of 20 November 2003, *J. Geophys. Res.*, *110*, A09S22, doi:10.1029/2004JA010924.
Förster, M., and N. Jakowski (2000), Geomagnetic storm effects on the topside ionosphere and plasmasphere: A compact tutorial and new results, *Surv. Geophys.*, *21*(1), 47–87, doi:10.1023/A:1006775125220.
Foster, J. C., et al. (2005), Multiradar observations of the polar tongue of ionization, *J. Geophys. Res.*, *110*, A09S31, doi:10.1029/2004JA010928.
Fuller-Rowell, T. J., M. V. Codrescu, R. J. Moffett, and S. Quegan (1994), Response of the thermosphere and ionosphere to geomagnetic storms, *J. Geophys. Res.*, *99*(A3), 3893–3914, doi:10.1029/93JA02015.
Gopalswamy, N., S. Yashiro, G. Michalek, H. Xie, R. P. Lepping, and R. A. Howard (2005), Solar source of the largest geomagnetic storm of cycle 23, *Geophys. Res. Lett.*, *32*, L12S09, doi:10.1029/2004GL021639.
Hajkowicz, L. (1991), Global onset and propagation of large-scale travelling ionospheric disturbances as a result of the great storm of 13 March 1989, *Planet. Space Sci.*, *39*(4), 583–593, doi:10.1016/0032-0633(91)90053-D.
Ho, C. M., A. J. Mannucci, L. Sparks, X. Pi, U. J. Lindqwister, B. D. Wilson, B. A. Iijima, and M. J. Reyes (1998), Ionospheric total electron content perturbations monitored by the GPS global network during two Northern Hemisphere winter storms, *J. Geophys. Res.*, *103*(A11), 26,409–26,420, doi:10.1029/98JA01237.
Hocke, K., and K. Schlegel (1996), A review of atmospheric gravity waves and traveling ionospheric disturbances, *Ann. Geophys.*, *14*(9), 917–940.
Hori, T., A. T. Y. Lui, S. Ohtani, P. C. Brandt, B. H. Mauk, R. W. McEntire, K. Maezawa, T. Mukai, Y. Kasaba, and H. Hayakawa (2006), Convection electric field in the near-Earth tail during the super magnetic storm of November 20–21, 2003, *Geophys. Res. Lett.*, *33*, L21107, doi:10.1029/2006GL027024.
Hunsucker, R. D. (1982), Atmospheric gravity waves generated in the high-latitude ionosphere: A review, *Rev. Geophys. Space Phys.*, *20*(2), 293–315.
Jakowski, N. (1996), TEC monitoring by using satellite positioning systems, in *Modern Ionospheric Science*, edited by H. Kohl, R. Rüster, and K. Schlegel, pp. 371–390, Eur. Geophys. Soc., Berlin.
Jakowski, N., and E. Putz (1986), Observations of large scale travelling ionospheric disturbances associated with geomagnetic storms, *Kleinheubacher Ber.*, *29*, 563–570.
Jakowski, N., E. Putz, and P. Spalla (1990), Ionospheric storm characteristics deduced from satellite radio beacon observations at three European stations, *Ann. Geophys.*, *8*(5), 343–352.
Jakowski, N., S. Schlüter, and E. Sardon (1999), Total electron content of the ionosphere during the geomagnetic storm on 10 January 1997, *J. Atmos. Sol. Terr. Phys.*, *61*(3–4), 299–307, doi:10.1016/S1364-6826(98)00130-8.
Jakowski, N., V. Wilken, and C. Mayer (2007), Space weather monitoring by GPS measurements on board CHAMP, *Space Weather*, *5*, S08006, doi:10.1029/2006SW000271.
Jakowski, N., M. M. Hoque, and C. Mayer (2011), A new global TEC model for estimating transionospheric radio wave propagation errors, *J. Geod.*, *85*, 965–974, doi:10.1007/s00190-011-0455-1.
Jakowski, N., A. Jungstand, K. Schlegel, H. Kohl, and K. Rinnert (1992), The ionospheric response to perturbation electric fields during the onset phase of geomagnetic storms, *Can. J. Phys.*, *70*(7), 575–581.
Jin, S., O. F. Luo, and P. Park (2008), GPS observations of the ionospheric F2-layer behavior during the 20th November 2003 geomagnetic storm over South Korea, *J. Geod.*, *82*(12), 883–892, doi:10.1007/s00190-008-0217-x.
Kataoka, R., D. H. Fairfield, D. G. Sibeck, L. Rastätter, M.-C. Fok, T. Nagatsuma, and Y. Ebihara (2005), Magnetosheath variations during the storm main phase on 20 November 2003: Evidence for solar wind density control of energy transfer to the magnetosphere, *Geophys. Res. Lett.*, *32*, L21108, doi:10.1029/2005GL024495.
Kersley, L., and K. Hughes (1989), On the distinction between large-scale and medium-scale atmospheric gravity waves, *Ann. Geophys.*, *7*, 459–462.
Maeda, S., and S. Handa (1980), Transmission of large-scale TIDs in the ionospheric F2-region, *J. Atmos. Terr. Phys.*, *42*, 853–859.
Mannucci, A. J., B. T. Tsurutani, M. A. Abdu, W. D. Gonzalez, A. Komjathy, E. Echer, B. A. Iijima, G. Crowley, and D. Anderson (2008), Superposed epoch analysis of the dayside ionospheric response to four intense geomagnetic storms, *J. Geophys. Res.*, *113*, A00A02, doi:10.1029/2007JA012732.

Mayer, C., N. Jakowski, C. Borries, T. Pannowitsch, and B. Belabbas (2008), Extreme ionospheric conditions over Europe observed during the last solar cycle, paper presented at 4th ESA Workshop on Satellite Navigation User Equipment Technologies, ESTEC, Noordwijk, Netherlands, 10-12 Dec.

Mishin, V., M. Foerster, T. Saifudinova, A. Bazarzhapov, Y. Karavaev, L. Sapronova, and S. Solovyev (2007), Spontaneous substorms and ordered type of magnetospheric disturbances during the superstorm of November 20, 2003, *Geomagn. Aeron.*, *47*(4), 429–441, doi:10.1134/S0016793207040032.

Oliver, W., Y. Otsuka, M. Sato, T. Takami, and S. Fukao (1997), Climatology of *F* region gravity waves propagation over the middle and upper atmosphere radar, *J. Geophys. Res.*, *102*, 14,499–14,512.

Oyama, S., and B. Watkins (2012), Generation of atmospheric gravity waves in the polar thermosphere in response to auroral activity, *Space Sci. Rev.*, *168*(1–4), 463–473, doi:10.1007/s11214-011-9847-z.

Prölss, G. W. (1995), Ionospheric F-region storms, in *Handbook of Atmospheric Electrodynamics*, vol. 2, edited by H. Volland, chap. 8, pp. 195–235, CRC Press, Boca Raton, Fla.

Prölss, G. W. (2006), Subauroral electron temperature enhancement in the nighttime ionosphere, *Ann. Geophys.*, *24*(7), 1871–1885, doi:10.5194/angeo-24-1871-2006.

Pulkkinen, A., O. Amm, and A. Viljanen (2003), Ionospheric equivalent current distributions determined with the method of spherical elementary current systems, *J. Geophys. Res.*, *108*(A2), 1053, doi:10.1029/2001JA005085.

Rice, D. D., R. D. Hunsucker, L. J. Lanzerotti, G. Crowley, and P. J. S. Williams (1988), An observation of atmospheric gravity wave cause and effect during October 1985 WAGS campaign, *Radio Sci.*, *23*, 919–930, doi:10.1029/RS023i006p00919.

Semeter, J., C. J. Heinselman, J. P. Thayer, R. A. Doe, and H. U. Frey (2003), Ion upflow enhanced by drifting F-region plasma structure along the nightside polar cap boundary, *Geophys. Res. Lett.*, *30*(22), 2139, doi:10.1029/2003GL017747.

Shimeis, A., C. Borries, C. Amory-Mazaudier, R. Fleury, A. Mahrous, A. Hassan, and S. Nawar (2015), TEC variations along an East Euro-African chain during 5th April 2010 geomagnetic storm, *Adv. Space Res.*, *55*(9), 2239–2247, doi:10.1016/j.asr.2015.01.005.

Shiokawa, K., G. Lu, Y. Otsuka, T. Ogawa, M. Yamamoto, N. Nishitani, and N. Sato (2007), Ground observation and AMIE-TIEGCM modeling of a storm-time traveling ionospheric disturbance, *J. Geophys. Res.*, *112*, A05308, doi:10.1029/2006JA011772.

Shiokawa, K., et al. (2003), Thermospheric wind during a storm-time large-scale traveling ionospheric disturbance, *J. Geophys. Res.*, *108*(A12), 1423, doi:10.1029/2003JA010001.

Tsugawa, T., A. Saito, and Y. Otsuka (2004), A statistical study of large-scale traveling ionospheric disturbances using the GPS network in Japan, *J. Geophys. Res.*, *109*, A06302, doi:10.1029/2003JA010302.

Viljanen, A., and L. Häkkinen (1997), IMAGE magnetometer network, in *Satellite-Ground Based Coordination Sourcebook, ESA Publ. SP-1198*, edited by M. Lockwood, M. Wild, and H. Opgenoorth, pp. 111–117, ESA, Noordwijk, Netherlands.

Volland, H. (1983), Dynamics of the disturbed ionosphere, *Space Sci. Rev.*, *34*, 327–335.

Williams, P., et al. (1988), Eiscat science the generation and propagation of atmospheric gravity waves observed during the worldwide atmospheric gravity-wave study (wags), *J. Atmos. Terr. Phys.*, *50*(4), 323–338, doi:10.1016/0021-9169(88)90018-9.

Yizengaw, E., and M. B. Moldwin (2005), The altitude extension of the mid-latitude trough and its correlation with plasmapause position, *Geophys. Res. Lett.*, *32*, L09105, doi:10.1029/2005GL022854.

Yizengaw, E., M. B. Moldwin, A. Komjathy, and A. J. Mannucci (2006), Unusual topside ionospheric density response to the November 2003 superstorm, *J. Geophys. Res.*, *111*, A02308, doi:10.1029/2005JA011433.